Mutual Interactions and Stability Analysis of Bipolar DC Microgrids

Saman Dadjo Tavakoli, Peng Zhang, *Senior Member, IEEE*, Xiaonan Lu, *Member, IEEE*, and Mohsen Hamzeh

***Abstract*—This paper presents an Multi-Input Multi-Output (MIMO) analysis to investigate the mutual interactions and small-signal stability of bipolar-type dc microgrids. Since bipolar dc microgrid is replete with power-electronic converters, its dynamics can not be understood unless the interactions among control systems of converters are properly investigated. To tackle the challenge, each converter in microgrid is modeled via an MIMO transfer matrix. Then, the MIMO models are combined together based on the interactions among the control systems of source and load converters. From this integrative MIMO model, the mutual interactions between various input-output pairs are quantified using Gershgorin Band theorem. Also, Singular Value Decomposition (SVD) analysis is carried out to estimate the frequency of unstable poles. Test results not only successfully validate the effectiveness of the MIMO method but also show that the control system of voltage balancer has a major impact on the overall stability of bipolar dc microgrid, making it a suitable location for applying damping systems.**

***Index Terms*—Bipolar dc microgrid, Gershgorin Band, MIMO analysis, small-signal stability, singular value decomposition, voltage balancer.**

I. Introduction

DC microgrids are steadily attracting attention mainly due to the proliferation of power-electronic loads and the dc nature of the majority of non-synchronous distributed energy resources (DERs) such as photovoltaic and wind generation systems [1]. In fact, since microgrids are replete with dc loads, it is technically and economically preferred to feed these loads directly by dc DERs avoiding multiple conversion of voltage from dc to ac and vice versa [2], [3]. Compared with the conventional dc microgrid, bipolar-type dc microgrid offers additional benefits. Due to its three-wire topology, two voltage levels are accessible to the loads, meaning heavy and light loads can be connected, respectively, to the higher and lower voltage levels. This not only reduces the ohmic loses, but also simplifies the converter topologies. However, there are several challenges associated with bipolar dc microgrids which require detailed investigations. Some of the challenges have been extensively investigated as they are common between conventional dc microgrids and bipolar dc microgrids. Hence, the same approach from conventional dc microgrids can be adopted. Nevertheless, there are some issues including grounding system, mutual interactions, and voltage instability which need to be specifically investigated for bipolar dc microgrids [4], [5].

The structure and operation principles of bipolar dc microgrid are studied in [4]. It is shown that bipolar dc microgrid is prone to unbalanced loading on L1-N and L2-N terminals. This calls for a voltage balancer to maintain the terminal voltages, L1-N and L2-N, at the nominal value under unbalanced loading [6]. Several converter topologies have been proposed for performing voltage balancing function [7], [8]. The operation of bipolar dc microgrid under unbalanced conditions has been studied using dc symmetrical component method [9]. Several power sharing strategies have been proposed in [10]. However, the mutual interactions and stability of bipolar dc microgrid are not properly addressed in current literature, and they require a detailed investigation because the L1-N and L2-N networks are not decoupled [5], [9].

The overall stability of conventional, unipolar dc microgrid is extensively studied in the recent literature. Using small-signal approximation, the stability of dc microgrid is studied by identifying the eigenvalues of the linearized system [11]. A nonlinear stability analysis of dc microgrid is provided in [12]; however, in both [11] and [12], the order of microgrid model is reduced and the detailed dynamic of converters are ignored. In [13], following to the linearization of the microgrid state-space equations, a fault-tolerant stabilization system is presented. The stability of the medium-voltage dc microgrid on ships is discussed in [14], in which a reduced-order model is employed. The eigen-analysis of a dc microgrid with parallel operation of multiple dc-dc buck converters is presented in [15]. However, all of the aforementioned literatures only apply to the conventional, unipolar dc microgrids, unable to explain the mutual interactions and detailed dynamic behavior of bipolar dc microgrid. Adopting a state-space approach, the stability of bipolar dc microgrid is modeled in [16]. Neither does it explain the mutual interactions between terminals of bipolar dc microgrid, nor can it analyze the small-signal behavior of bipolar dc microgrid under unbalanced loading.

Manuscript received August 28, 2018; revised April 10, 2019; accepted July 5, 2019. Date of publication December 30, 2019; date of current version October 22, 2019. This work was supported by the U.S. National Science Foundation under Grant Nos. 1647209 and 1611095, and by the European Unions Horizon 2020 Research and Innovation Programme under the Marie Sklodowska-Curie Grant No. 765585.

S. D. Tavakoli is with Department of Electrical Engineering, Universitat Politecnica de Catalunya, Barcelona, Catalunya 08034, Spain.

P. Zhang (corresponding author, email: P.Zhang@stonybrook.edu) is with Department of Electrical and Computer Engineering, Stony Brook University, Stony Brook, NY 11794-2350, USA.

X. N. Lu is with Department of Electrical and Computer Engineering, Temple University, Philadelphia, PA 19122, USA.

M. Hamzeh is with Department of Electrical Engineering, University of Tehran, Tehran, Iran.

DOI: 10.17775/CSEEJPES.2018.00870

To bridge the gap, this paper proposes an MIMO analysis which accurately captures the small-signal dynamics of bipolar dc microgrids and the mutual interactions between L1N and L2N terminals. The importance of the MIMO approach lies in the fact that the main cause of instability in microgrids is the interactions among the control systems of source and load converters. The main contributions of this paper include: 1) The MIMO transfer matrices of the major components in bipolar dc microgrid are derived; 2) The MIMO transfer matrices are then combined together making one MIMO system with desired inputs and outputs which represents the overall dynamics of bipolar dc microgrid; 3) The mutual interactions between various inputs and outputs are identified and sensitivities are established; 4) The degree of coupling between L1N and L2N terminals for the unbalanced bipolar dc microgrid is quantified using Gershgorin Band theorem; 5) A Relative Gain Array (RGA) analysis is conducted to illustrate the mutual interactions between control loops of converters; 6) The frequency of unstable poles is estimated by SVD analysis; 7) Our MIMO approach reveals that the dominant poles of the microgrid are significantly affected by the dynamics of the voltage balancer.

II. MIMO Analysis of Bipolar DC Microgrid

A. Modeling Method

In this section, the MIMO modeling of a typical bipolar dc microgrid shown in Fig. 1 is presented. The Gershgorin Band theorem and SVD analysis are then applied to understand the mutual interactions and stability of the microgrid.

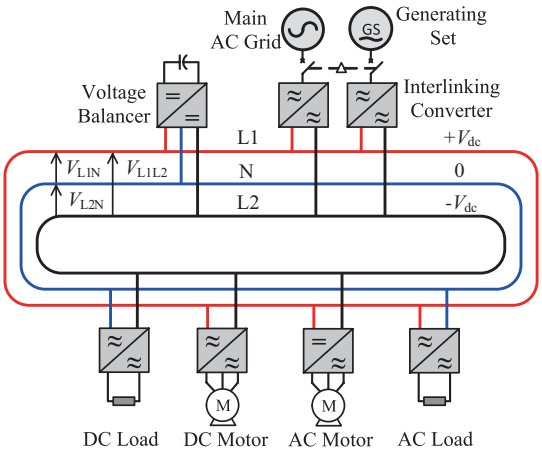

Fig. 1. Ring-type bipolar dc microgrid.

In a conventional dc microgrid, the voltage of the main dc bus is regulated via voltage control loops of source-side converters. Unfortunately, this voltage acts as disturbance to the control loops of load-side converters. Moreover, the input currents of the load-side converters act as disturbances to the control loops of source-side converters. The mutual interactions between source-side and load-side converters are shown in Fig. 2. It is important to notice that, the load-side converters have also influence on each other. For instance, a change in the load current i_{load1} would also change i_{in1}. Subsequently, a change in i_{in1} results in variations in v_{dc} since i_{in1} is disturbance to the control system regulating v_{dc}. Finally, the variations in v_{dc} would change the output voltage v_{o2}. Thus, if the interactions among voltage and current signals of all converters are properly mapped, the small-signal stability of microgrid can be discovered.

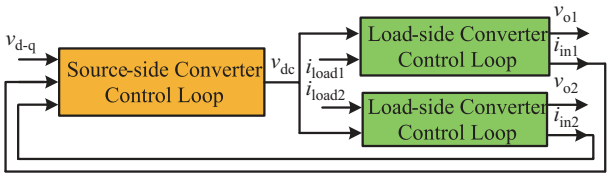

Fig. 2. The interactions among the control loops of converters.

In a bipolar dc microgrid, the control loops of converters interact through L1-N and L2-N voltages. In fact, v_{L1L2} is maintained via interlinking converter. Then, the voltage balancer regulates and balances v_{L1N} and v_{L2N}. These voltages are disturbances to the control loops of the load-side converters. Furthermore, any load disturbance on the L1-N terminal would have impact on the L2-N terminal voltage and vice versa. This is the mutual coupling between the L1N and L2N terminals which complicates the stability analysis. It is worth mentioning that the line impedances are ignored to gain a better insight since the primary aim of this paper is to show the mutual interactions between L1N and L2N terminals and the impact of voltage balancer on stability. However, any component or impedance can be also considered in this analysis.

The small-signal model of bipolar dc microgrid is presented in Fig. 3(a). Each block in this diagram represents a set of major power equipment in bipolar dc microgrid. A conventional inverter is used as interlinking converter that regulates the dc line-to-line (L1–L2) voltage. The high power loads, such as ac or dc motor drives, are connected to v_{L1L2}. This voltage is then split to v_{L1N} and v_{L2N} to supply low power loads.

Each block in Fig. 3(a) is an MIMO system defined by an MIMO transfer matrix. On the source side, the generating unit or ac main grid is considered to supply the bipolar dc microgrid through the ac/dc interlinking converter. The v_{L1L2} does not directly interact with the control loops of the loads connected across L1N and L2N terminals. It is a disturbance to the control system of the voltage balancer and the loads connected across L1L2 terminal. All loads, regardless of their types, should be modeled via transfer matrix in which the input voltage and output current (load current) are the input variables; and the output voltage (load voltage) and input current are the output variables. In fact, it does not matter that the load is a dc/dc converter or a dc/ac motor drive as what we need for MIMO analysis is the input/output voltage and current variables.

The voltage balancer is a crucial converter indispensable to the proper function of bipolar dc microgrid. While the inverter maintains the voltage across L1L2 (v_{L1L2}), the voltage balancer operates to make the voltage difference across L1N and L2N (v_{L1N}–v_{L2N}) equal to zero.

As shown in Fig. 3(a), the interaction among L1N and L2N loads occurs through this converter. Notice that the sum of the

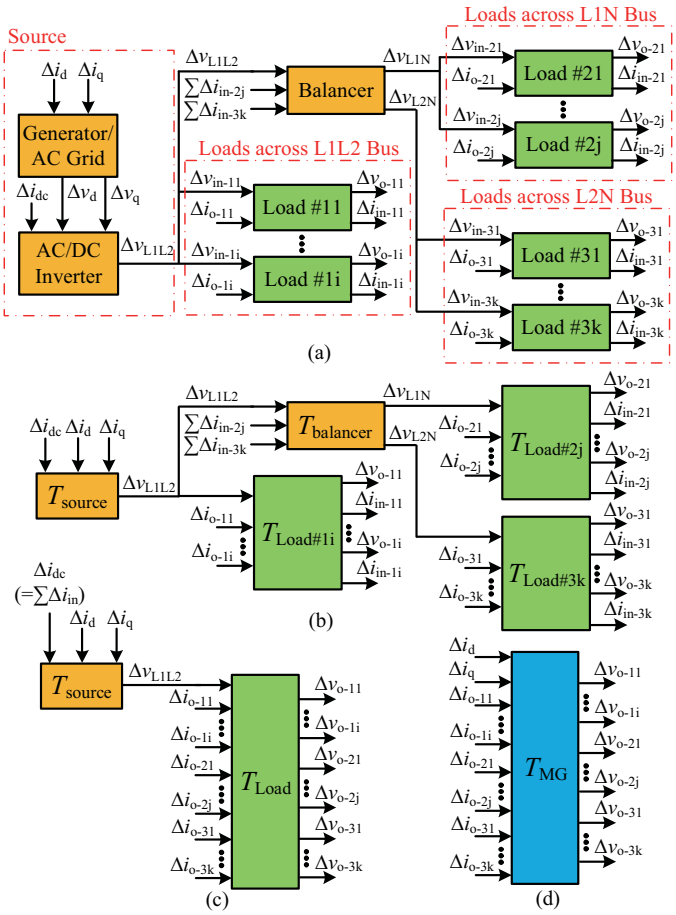

Fig. 3. Bipolar dc microgrid small-signal model; various stages to obtain one overall MIMO model for the entire bipolar dc microgrid; (a) small-signal model of microgrid where each component is presented by an MIMO model, (b) the individual MIMO models are locally combined to build blocks of loads and a block of source, (c) the MIMO models are further combined to form load and source sub-systems, and (d) overall MIMO model of the microgrid.

input currents of the loads connected across L1N bus, as well as the loads connected across L2N bus, act as disturbance to the voltage control loop of the balancer.

Three groups of loads are connected to the microgrid: L1L2 loads (Load #11 to Load #1i), L1N loads (Load #21 to Load #2j), and finally L2N loads (Load #31 to Load #3k). The subsystems presented in Fig. 3(a) can be combined to achieve the system shown in Fig. 3(b). The transfer matrix $\boldsymbol{T}_{\text{source}}$ represents the complete generating sets, including the ac/dc inverter.

The system presented in Fig. 3(b) can be seen as two subsystems of source ($\boldsymbol{T}_{\text{source}}$) and load ($\boldsymbol{T}_{\text{Load}}$). This is shown in Fig. 3(c). Although $\boldsymbol{T}_{\text{balancer}}$ is neither load nor source, it is integrated into the load subsystem. The final step is to combine the two subsystems to reach the final MIMO system $\boldsymbol{T}_{\text{MG}}$ which is presented in Fig. 3(d).

The destabilizing impact of constant power loads (CPL) is also considered in the MIMO analysis. If the output voltage of a load-side converter is tightly regulated, the converter behaves as a CPL with a negative incremental resistance that reduces the stability margins [17]. For the constant output voltage and load, the output power of the converter is also constant at $P_{\text{out}} = V_{\text{out}}^2/R_{\text{Load}}$. This means that for a given efficiency, the input power of the converter is also constant at P. The input current, i_{in}, and voltage, v_{in}, of the converter have the following relation [18], [19],

$$i_{\text{in}} = \frac{P}{v_{\text{in}}} \tag{1}$$

Hence, the small-signal variations of input current due to a change in input voltage can be expressed as,

$$\triangle i_{\text{in}} = -\frac{P}{V_{\text{in}}^2} \times \triangle v_{\text{in}} \tag{2}$$

This means that for a step increase in input voltage, the input current reduces by a magnitude of P/V_{in}^2.

Once $\boldsymbol{T}_{\text{MG}}$ is computed, the stability and mutual interactions between various input-output pairs can be studied. In order to reveal mutual interactions and the degree of coupling, the Gershgorin circle (Gershgorin band) is used. The Gershgorin band identifies a region in the complex plane that contains all eigenvalues of a complex matrix. For the given operating point, $\boldsymbol{T}_{\text{MG}}(jw)$ is a complex matrix whose eigenvalues fall on the union of circles with center at $\boldsymbol{T}_{\text{MG}}(i,i)$ with radius

$$\sum_{j=1, j\neq i}^{4} |\boldsymbol{T}_{\text{MG}}(i,j)| \tag{3}$$

and on the circles with center at $\boldsymbol{T}_{\text{MG}}(j,j)$ with radius

$$\sum_{i=1, i\neq j}^{3} |\boldsymbol{T}_{\text{MG}}(i,j)| \tag{4}$$

The above mentioned circles are super imposed on the Nyquist diagrams of $\boldsymbol{T}_{\text{MG}}(i,i)$. Note that we are not interested in knowing the system stability from the result Nyquist diagrams; instead, we are looking for the regions occupied by Gershgorin bands. If the Gershgorin bands are thin, then $\boldsymbol{T}_{\text{MG}}(s)$ is diagonally dominant which can be interpreted as a weakly coupled MIMO system. In other words, the Gershgorin theorem gives information on how diagonal the MIMO transfer matrix $\boldsymbol{T}_{\text{MG}}(s)$ is. The more diagonal it is, the weaker the interactions between L1N and L2N.

The frequency-dependent RGA analysis can be utilized as a complementary to the Gershgorin theorem. RGA analysis indicates how the control loops of converters mutually interact for various frequency ranges. The higher RGA values are associated with the stronger interactions between control loops of converters. In control engineering, RGA is defined as,

$$RGA(\boldsymbol{T}_{\text{MG}}(jw)) \triangleq \boldsymbol{T}_{\text{MG}}(jw) \times ((\boldsymbol{T}_{\text{MG}}(jw))^{-1})^{\text{T}} \tag{5}$$

where the transfer matrix $\boldsymbol{T}_{\text{MG}}(s)$ is multiplied by its inverse transposed matrix at the frequency of interest.

The Gershgorin theorem reveals the degree of coupling between input-output pairs; however, it gives no information about how large the system response is for specific inputs. In MIMO systems, Singular Value Decomposition (SVD) provides a system frequency response which includes all mutual interactions. The SVD analysis shows how much amplification we can get with a vector of inputs.

The singular values of the microgrid transfer matrix, $\boldsymbol{T}_{\rm MG}(s)$, for $s = jw$ is denoted as

$$\sigma_i(\boldsymbol{T}_{\rm MG}(jw)) = \sqrt{\lambda_i\ (\boldsymbol{T}_{\rm MG}(jw)^{\rm H}\boldsymbol{T}_{\rm MG}(jw))} \tag{6}$$

where $\lambda_i(\cdot)$ denotes the ith eigenvalue of the matrix, and $\boldsymbol{T}_{\rm MG}(jw)^{\rm H}$ is a conjugate transpose (Hermitian adjoint) matrix. The maximum amplification that the input vector can experience is given by the maximum singular value $\overline{\sigma}(\boldsymbol{T}_{\rm MG}(jw))$ and the minimum amplification by the minimum singular value $\underline{\sigma}(\boldsymbol{T}_{\rm MG}(jw))$.

B. Formation of Microgrid MIMO Equations

The aim of this section is to show how to implement the modeling method to build the MIMO model of a bipolar dc microgrid.

Without loss of generality, the MIMO modeling method is applied to the bipolar dc microgrid shown in Fig. 4. The given microgrid comprises three loads, a conventional inverter, and a voltage balancer. The transfer matrices of the loads should have the following form:

$$\begin{bmatrix}\triangle v_{\rm o}\\ \triangle i_{\rm in}\end{bmatrix} = \boldsymbol{T}_{\rm Load}\begin{bmatrix}\triangle v_{\rm in}\\ \triangle i_{\rm o}\end{bmatrix} \tag{7}$$

where $\boldsymbol{T}_{\rm Load}$ is a 2×2 transfer matrix, $\triangle i_{\rm o}$ and $\triangle v_{\rm o}$ are, respectively, output current and voltage, and $\triangle i_{\rm in}$ and $\triangle v_{\rm in}$ are input current and voltage, respectively. Equation (7) is generic and applies to any type of load such as a conventional dc/dc converter or dc/ac electric motor drive.

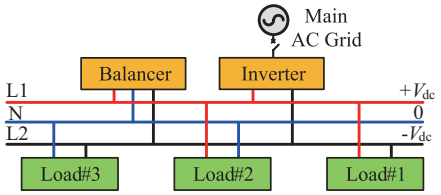

Fig. 4. Bipolar dc microgrid for MIMO stability analysis.

The control loop of a dc/dc converter is shown in Fig. 5(a). The output current (load current), $\triangle i_{\rm o}$, and input voltage, $\triangle v_{\rm in}$, are disturbance to the voltage control loop. There are five plant transfer functions to be established, including $T_{\rm vd}(s)$, $T_{\rm vv}(s)$, $T_{\rm iv}(s)$, $T_{\rm ii}(s)$, and $T_{\rm vi}(s)$, and one PI controller $T_{\rm c}(s)$. Through state-space averaging, the small-signal

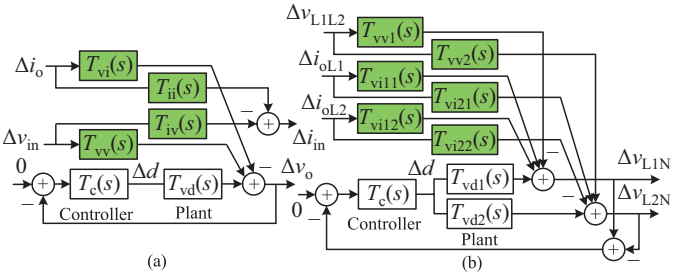

Fig. 5. The control system of (a) the conventional dc/dc converters, and (b) the voltage balancer.

equations for common dc/dc converters can be expressed as

$$\dot{\triangle\boldsymbol{x}} = \boldsymbol{A}_{\rm ave}\triangle\boldsymbol{x} + \boldsymbol{B}_{\rm ave}\triangle\boldsymbol{u} + [(\boldsymbol{A}_1 - \boldsymbol{A}_2)\boldsymbol{X} + (\boldsymbol{B}_1 - \boldsymbol{B}_2)\boldsymbol{U}]\triangle d \tag{8}$$

$$\triangle\boldsymbol{y} = \boldsymbol{C}_{\rm ave}\triangle\boldsymbol{x} + \boldsymbol{E}_{\rm ave}\triangle\boldsymbol{u} + [(\boldsymbol{C}_1 - \boldsymbol{C}_2)\boldsymbol{X} + (\boldsymbol{E}_1 - \boldsymbol{E}_2)\boldsymbol{U}]\triangle d \tag{9}$$

where $\boldsymbol{x}$ contains capacitor voltages and inductor currents and $\boldsymbol{u}$ contains input dc voltage and output current. The matrices $\boldsymbol{X}$ and $\boldsymbol{U}$ contain the steady-state values of state variables and inputs, respectively. $\boldsymbol{A}_1$ to $\boldsymbol{E}_1$ and $\boldsymbol{A}_2$ to $\boldsymbol{E}_2$ are coefficient matrices with constant elements. The averaged matrices are indicated with subscript ave. The control signal is duty cycle, d, and the desirable output variables, including input current and output voltage, are in the vector $\boldsymbol{y}$. Using (8) and (9), the transfer functions of a conventional dc/dc converter can be obtained from

$$\triangle\boldsymbol{x} = (s\boldsymbol{I} - \boldsymbol{A}_{\rm ave})^{-1}((\boldsymbol{A}_1 - \boldsymbol{A}_2)\boldsymbol{X} + (\boldsymbol{B}_1 - \boldsymbol{B}_2)\boldsymbol{U})\triangle d \tag{10}$$

$$\triangle\boldsymbol{x} = (s\boldsymbol{I} - \boldsymbol{A}_{\rm ave})^{-1}\boldsymbol{B}_{\rm ave}\triangle\boldsymbol{u} \tag{11}$$

For instance, in case of a dc/dc boost converter, the capacitor voltage and inductor current would be equal to, respectively, output voltage and input current. Hence,

$$\triangle\boldsymbol{x} = [\triangle v_{\rm o}, \triangle i_{\rm in}]^{\rm T} \text{ and } \triangle\boldsymbol{u} = [\triangle v_{\rm in}, \triangle i_{\rm o}]^{\rm T}$$

$$\boldsymbol{A}_1 = \begin{bmatrix}0 & -1/CR\\ 0 & 0\end{bmatrix},\ \boldsymbol{B}_1 = \begin{bmatrix}1/L & 0\\ 0 & -1/C\end{bmatrix}$$

$$\boldsymbol{A}_2 = \begin{bmatrix}1/C & -1/CR\\ 0 & -1/L\end{bmatrix},\ \boldsymbol{B}_2 = \begin{bmatrix}1/L & 0\\ 0 & -1/C\end{bmatrix}$$

$$\boldsymbol{A}_{\rm ave} = d\boldsymbol{A}_1 + (1-d)\boldsymbol{A}_2,\ \boldsymbol{B}_{\rm ave} = d\boldsymbol{B}_1 + (1-d)\boldsymbol{B}_2$$

where C, L, and R are, respectively, output capacitor, inductor, and load resistance of the boost converter. The plant transfer function $T_{\rm vd}(s)$ can be obtained from (10) and the rest of transfer functions are obtained from (11) as follows:

$$T_{\rm vd} = [1,0]\times[(s\boldsymbol{I} - \boldsymbol{A}_{\rm ave})^{-1}((\boldsymbol{A}_1 - \boldsymbol{A}_2)\boldsymbol{X} + (\boldsymbol{B}_1 - \boldsymbol{B}_2)\boldsymbol{U})]$$

$$\begin{bmatrix}T_{\rm vv} & -T_{\rm vi}\\ -T_{\rm iv} & T_{\rm ii}\end{bmatrix} = [(s\boldsymbol{I} - \boldsymbol{A}_{\rm ave})^{-1}\boldsymbol{B}_{\rm ave}]$$

After computing the transfer functions of Fig. 5(a), the elements of $\boldsymbol{T}_{\rm Load}$ are readily available,

$$\boldsymbol{T}_{\rm Load} = \begin{bmatrix}\dfrac{T_{\rm vv}}{1 + T_{\rm c}T_{\rm vd}} & \dfrac{-T_{\rm vi}}{1 + T_{\rm c}T_{\rm vd}}\\ -T_{\rm iv} & T_{\rm ii}\end{bmatrix} \tag{12}$$

The first row of $\boldsymbol{T}_{\rm Load}$, which is related to the output voltage, has a closed loop form. This reflects that the converter is operating under voltage control mode. The negative value of $T_{\rm iv}$ is also consistent with the concept of CPL.

The transfer matrix of the voltage balancer, $\boldsymbol{T}_{\rm balancer}$, can be obtained using the same state-space averaging method as described above. The topology and operating mode of the voltage balancer have been extensively described in [6], [20]. So, we only present its control system in Fig. 5(b). Here again, the disturbances to the control loop of voltage balancer are load currents, $i_{\rm oL1}$ and $i_{\rm oL2}$, and the input voltage, $v_{\rm L1L2}$.

The control system of the balancer operates to maintain the difference between the output voltages, v_{L1N} and v_{L2N}, at zero. v_{L1L2} is controlled via an inverter. The control system has eight plant transfer functions and one PI controller. The output capacitor voltages and inductor current are the elements of $\triangle \boldsymbol{x}$. The capacitor voltages are equal to L1N and L2N voltages. Therefore,

$$\triangle \boldsymbol{x} = [\triangle v_{\mathrm{L1N}}, \triangle v_{\mathrm{L2N}}, \triangle i_{\mathrm{L}}]^{\mathrm{T}}$$
$$\triangle \boldsymbol{u} = [\triangle i_{\mathrm{oL1}}, \triangle i_{\mathrm{oL2}}, \triangle v_{\mathrm{L1L2}}]^{\mathrm{T}}$$
$$\boldsymbol{A}_1 = \begin{bmatrix} -1/2Cr_{\mathrm{c}} & -1/2Cr_{\mathrm{c}} & 1/2C \\ -1/2Cr_{\mathrm{c}} & -1/2Cr_{\mathrm{c}} & -1/2C \\ -1/2L & 1/2L & (r_{\mathrm{c}})/2L \end{bmatrix}$$
$$\boldsymbol{B}_1 = \begin{bmatrix} -1/2C & 1/2C & 1/2Cr_{\mathrm{c}} \\ -1/2C & -1/2C & 1/2Cr_{\mathrm{c}} \\ r_{\mathrm{c}}/2L & -r_{\mathrm{c}}/2L & 1/2L \end{bmatrix}$$

where L, C, and r_{c} are inductor, output capacitor, and the associated equivalent series resistance, respectively (see [20] for the balancer topology). $\boldsymbol{A}_2$ and $\boldsymbol{B}_2$ are equal to $\boldsymbol{A}_1$ and $\boldsymbol{B}_1$, respectively; except that $\boldsymbol{B}_1(3,3) = -\boldsymbol{B}_2(3,3)$. The plant transfer functions can be obtained from (10) and (11) as follows:

$$\begin{bmatrix} T_{\mathrm{vd1}} \\ T_{\mathrm{vd2}} \end{bmatrix} = \begin{bmatrix} 1,0,0 \\ 0,1,0 \end{bmatrix}$$
$$[(s\boldsymbol{I} - \boldsymbol{A}_{\mathrm{ave}})^{-1}((\boldsymbol{A}_1 - \boldsymbol{A}_2)X + (\boldsymbol{B}_1 - \boldsymbol{B}_2)\boldsymbol{U})]$$
$$\begin{bmatrix} -T_{\mathrm{vi11}} & T_{\mathrm{vi12}} & T_{\mathrm{vv1}} \\ T_{\mathrm{vi21}} & -T_{\mathrm{vi22}} & T_{\mathrm{vv2}} \\ 0 & 0 & 0 \end{bmatrix} = \begin{bmatrix} 1,1,1 \\ 1,1,1 \\ 0,0,0 \end{bmatrix}$$
$$[(s\boldsymbol{I} - \boldsymbol{A}_{\mathrm{ave}})^{-1}\boldsymbol{B}_{\mathrm{ave}}]$$

The balancer is then described by the following equation set,

$$\begin{bmatrix} \triangle v_{\mathrm{L1N}} \\ \triangle v_{\mathrm{L2N}} \end{bmatrix} = \boldsymbol{T}_{\mathrm{balancer}} \begin{bmatrix} \triangle i_{\mathrm{oL1}} \\ \triangle i_{\mathrm{oL2}} \\ \triangle v_{\mathrm{L1L2}} \end{bmatrix} \tag{13}$$

The small-signal model of ac/dc inverter which interlinks the ac grid/synchronous generator to the bipolar dc microgrid is presented in Fig. 6. The linearized active power equation is given by

$$\triangle p_{\mathrm{s}} = \frac{3}{2} I_{\mathrm{d}} \triangle v_{\mathrm{d}} + \frac{3}{2} V_{\mathrm{d}} \triangle i_{\mathrm{d}} \tag{14}$$

where I_{d} and V_{d} are steady state current and voltage, respectively. The constant gains K_1 to K_5 presented in Fig. 6(b) are due to the linearization

$$K_1 = \frac{2}{3V_{\mathrm{d}}}, K_2 = \frac{3V_{\mathrm{d}}}{2},$$
$$K_3 = \frac{1}{2V_{\mathrm{L1L2}}}, K_4 = \frac{I_{\mathrm{d}}}{V_{\mathrm{d}}}, K_5 = \frac{3I_{\mathrm{d}}}{2}$$

The inverter operates under the dc-link voltage control mode, meaning v_{L1L2} is regulated by a voltage control loop, which in fact, controls the stored energy of the dc-link capacitor. As electrical energy is proportional to the square of voltage across capacitor, it is easier to regulate voltage using its square value. The voltage control loop generates the active power reference of the inverter, $p_{\mathrm{s}}^{\mathrm{ref}}$, which is fed to the current controller in dq frame [21].

In the grid-connected mode, the inverter exchanges power with the ac grid and maintains v_{L1L2} at the $V_{\mathrm{L1L2}}^{\mathrm{ref}}$ value. The ac-side voltage and frequency of the inverter are imposed by the ac grid so it injects the active power of $p_{\mathrm{s}}^{\mathrm{ref}}$ to the ac grid. Since the inverter operates in dc-link voltage control mode, only the d-axis control system, which is related to v_{d} and i_{d}, is of importance.

The transfer function relating $\triangle v_{\mathrm{L1L2}}$ to $\triangle v_{\mathrm{d}}$ can be obtained by applying Mason Gain Formula to the control system shown in Fig. 6(b). The dc output current of the inverter, $\triangle i_{\mathrm{dc}}$, also acts as disturbance to the $\triangle v_{\mathrm{L1L2}}$. The inverter output current, $\triangle i_{\mathrm{L1L2}}$, is simply the summation of the dc-link capacitor C current $\triangle i_{\mathrm{c}}$ and $\triangle i_{\mathrm{dc}}$. Moreover, $\triangle i_{\mathrm{dc}}$ is the current injected into the dc grid by the inverter, so it is equal to all load currents. Since the main ac grid is stiff compared to a dc microgrid, we can ignore the dynamics of the ac side. Therefore, the source transfer function will have the following equation:

$$\triangle v_{\mathrm{L1L2}}(s) = \boldsymbol{T}_{\mathrm{source}}(s) \begin{bmatrix} \triangle v_{\mathrm{d}}(s) \\ \triangle i_{\mathrm{dc}}(s) \end{bmatrix} \tag{15}$$

Referring to Fig. 3, the transfer matrices given by (7), (13), and (15) can be combined together to formulate the small-signal stability of the bipolar dc microgrid presented in Fig. 4. Note that $\triangle v_{\mathrm{L1N}}$ and $\triangle v_{\mathrm{L2N}}$, regulated by the voltage balancer, are disturbance to the control loops of the loads. However, the input disturbance of the voltage balancer are $\triangle i_{\mathrm{oL1}}$ and $\triangle i_{\mathrm{oL2}}$, which are the sum of the output currents of the loads connected to, respectively, L1N bus and L2N bus.

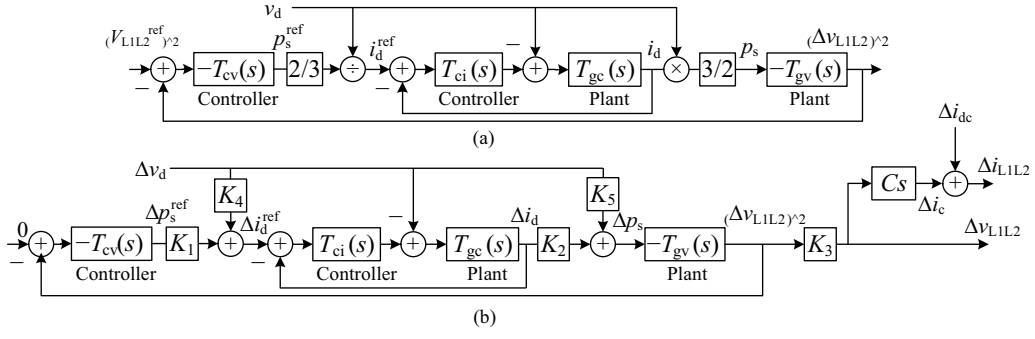

Fig. 6. Control system of an ac/dc inverter in dc-link voltage control mode, (a) non-linear model, and (b) linear model.

Considering this, the transfer matrix of the voltage balancer which includes the dynamics of the loads connected to L1N and L2N bus can be written as,

$$\begin{bmatrix} \triangle v_{\mathrm{L1N}} \\ \triangle v_{\mathrm{L2N}} \end{bmatrix} = \boldsymbol{T}_{\mathrm{balancer}} \begin{bmatrix} \triangle i_{\mathrm{o2}} \\ \triangle i_{\mathrm{o3}} \\ \triangle v_{\mathrm{L1L2}} \end{bmatrix} \tag{16}$$

where $\triangle v_{\mathrm{L1N}}$ and $\triangle v_{\mathrm{L2N}}$ are the output voltages of the balancer, $\triangle i_{\mathrm{o2}}$ and $\triangle i_{\mathrm{o3}}$ are the load currents, and $\triangle v_{\mathrm{L1L2}}$ is the inverter dc-link voltage. The coupling effects between the control loops of L1N and L2N bus can be observed by (16). In fact, using (16), the impact of load change on L2N bus can be observed on the output voltage of the load connected to L1N bus. Next, the balancer transfer matrix can be integrated into the load transfer matrix (see Fig. 3(c)),

$$\begin{bmatrix} \triangle v_{\mathrm{o1}} \\ \triangle v_{\mathrm{o2}} \\ \triangle v_{\mathrm{o3}} \end{bmatrix} = \boldsymbol{T}_{\mathrm{Load}} \begin{bmatrix} \triangle i_{\mathrm{o1}} \\ \triangle i_{\mathrm{o2}} \\ \triangle i_{\mathrm{o3}} \\ \triangle v_{\mathrm{L1L2}} \end{bmatrix} \tag{17}$$

Finally, the dynamic of the inverter is integrated into (17) to establish the microgrid MIMO model. Note that $\triangle i_{\mathrm{dc}}$ is not an independent variable, it is the summation of all load currents.

$$\begin{bmatrix} \triangle v_{\mathrm{o1}} \\ \triangle v_{\mathrm{o2}} \\ \triangle v_{\mathrm{o3}} \end{bmatrix} = \boldsymbol{T}_{\mathrm{MG}} \begin{bmatrix} \triangle i_{\mathrm{o1}} \\ \triangle i_{\mathrm{o2}} \\ \triangle i_{\mathrm{o3}} \\ \triangle v_{d} \end{bmatrix} \tag{18}$$

where the load currents $\triangle i_{\mathrm{o1}}$, $\triangle i_{\mathrm{o2}}$, and $\triangle i_{\mathrm{o3}}$ and inverter d-axis voltage $\triangle v_d$ are connected to the load output voltages $\triangle v_{\mathrm{o1}}$, $\triangle v_{\mathrm{o2}}$, and $\triangle v_{\mathrm{o1}}$ through the transfer matrix $\boldsymbol{T}_{\mathrm{MG}}(s)$. Obviously, $\boldsymbol{T}_{\mathrm{MG}}(s)$ has an order of 3 by 4, which provides a suitable mean for mutual interaction analysis.

III. Results and Discussion

The MIMO method is extensively tested on the bipolar dc microgrid shown in Fig. 4 which has a nominal line to neutral voltage of 400 Vdc and line to line voltage of 800 Vdc. The Load#1 is a dc/dc boost converter loaded by a resistive load; while Load#2 and Load#3 are dc/dc buck converters which are again loaded by resistive loads. The specifications of the components are given by Table I and the control systems are shown in Fig. 5(a), Fig. 5(b), and Fig. 6.

TABLE I
BIPOLAR DC MICROGRID PARAMETERS

Item	Specifications
Load#1	$V_{\mathrm{out}} = 1000$ V, $P_{\mathrm{nom}} = 10$ kW, $L = 3.7$ mH, $C = 10$ μF, $f_{\mathrm{s}} = 40$ kHz
Load#2	$V_{\mathrm{out}} = 100$ V, $P_{\mathrm{nom}} = 2$ kW, $L = 938$ μH, $C = 313$ μF, $f_{\mathrm{s}} = 40$ kHz
Load#3	$V_{\mathrm{out}} = 200$ V, $P_{\mathrm{nom}} = 8$ kW, $L = 625$ μH, $C = 625$ μF, $f_{\mathrm{s}} = 40$ kHz
Inverter	$P_{\mathrm{nom}} = 20$ kW, $V_{\mathrm{L1L2}} = 800$ V, $L = 2$ mH, $r_L = 2$ mΩ, $C = 20$ mF, $f_{\mathrm{s}} = 4$ kHz
Balancer	$V_{\mathrm{out}} = 2 \times 400$ V, $P_{\mathrm{nom}} = 3$ kW, $L = 600$ μH, $C = 5$ mF, $f_{\mathrm{s}} = 40$ kHz
AC Grid	$v_{\mathrm{L-L}} = 380Vrms$, $f = 60$ Hz

Two types of studies are performed: one for understanding both local and mutual interactions and their impacts on the stability of a bipolar dc microgrid, the other for gaining insights on the impact of voltage balancer on the microgrid stability.

A. Interactions in Bipolar DC Microgrid

1) Local Interactions

This study is to show how interactions can cause a locally stable converter to become unstable when connected to the microgrid.

In this case, the Load#1, Load#2, and Load#3 consume power of, respectively, 10 kW, 2 kW, and 2 kW, which means that the microgrid is balanced. In steady state, the voltage balancer neither absorbs, nor injects power to L1N or L2N bus. The total load of 14 kW is supplied by the inverter.

Before analyzing the local interactions, it is useful to show the consistency of (7) with the concept of CPL. The element (2,1) of $\boldsymbol{T}_{\mathrm{Load}}$ given by (7) indicates the relation between input current and input voltage, which must be consistent with (2). For instance, for a step increase in the input voltage of Load#2, its input current should decrease by 0.0125 A. This is indicated in Fig. 7.

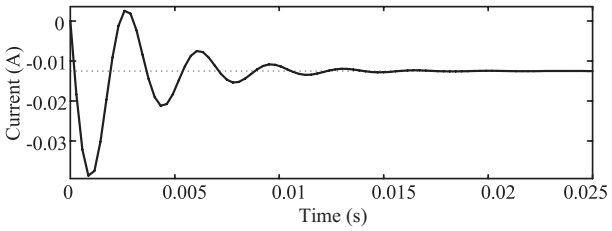

Fig. 7. The step response of $\boldsymbol{T}_{\mathrm{Load2}}(2,1)$ which indicates the relation between the input current and input voltage.

The interactions between the control loops of the converters can be understood by examination of the converters' transfer matrices before and after connecting to the microgrid. Considering Load#3, the small-signal relation between the output current (load current) and output voltage ($\triangle v_{\mathrm{o3}}/\triangle i_{\mathrm{o3}}$) is given by $\boldsymbol{T}_{\mathrm{Load3}}(1,2)$ before the converter is connected to the microgrid. The pole-zero map of $\boldsymbol{T}_{\mathrm{Load3}}(1,2)$ is shown in Fig. 8(a), which represents a stable system. However, when this converter (Load#3) is connected to the microgrid, the interactions among the control loops of other converters inflict unwanted dynamics into the control loop of Load#3. This is calculated by (18), $\boldsymbol{T}_{\mathrm{MG}}(3,3)$, which represents an unstable system with right-hand poles as shown in Fig. 8(b). Hence, the new poles and zeros are due to the interactions between Load#3 and other converters in the microgrid.

Therefore, if we ignore the dynamics of the input voltage source, the control system of Load#3 is stable; however, if the dynamics of the input source are considered, the converter becomes unstable. This also happens for Load#2 and it becomes unstable while connected to the microgrid. The response of v_{o2} for a step increase in i_{o2} is shown in Fig. 9. While the dynamics of the input voltage source is ignored, the converter remains stable and rejects the disturbance of i_{o2}, but it becomes unstable if the dynamics of the microgrid are included.

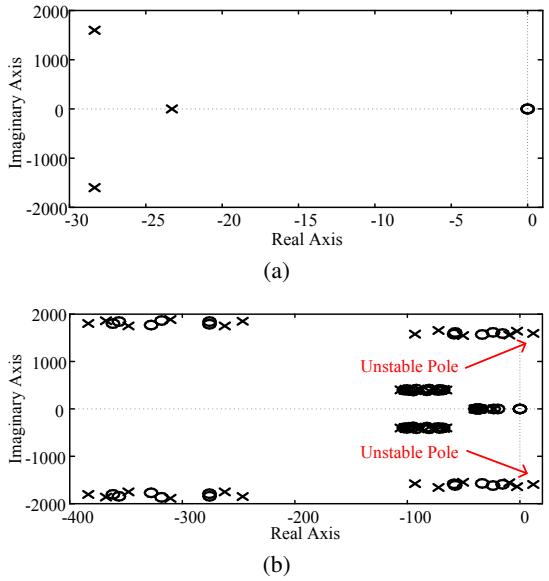

Fig. 8. Pole-zero map of $\triangle v_{o3}/\triangle i_{o3}$, (a) before connecting to the microgrid, and (b) after connecting to the microgrid.

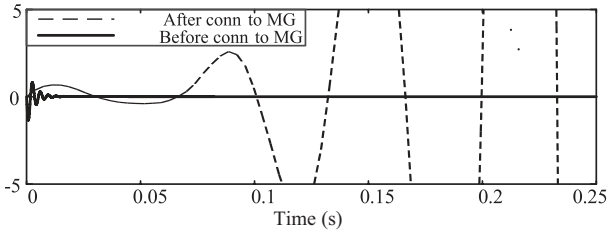

Fig. 9. The step response of $\triangle v_{o2}/\triangle i_{o2}$ before and after connecting to the microgrid.

2) Mutual Interactions

This study is conducted to understand the followings: 1) how a load change on L1N bus impacts the output voltage of the converter connected to L2N bus; 2) how the Gershgorin bands explain the degree of coupling between various input-output pairs as the microgrid becomes more unbalanced; and finally 3) how the SVD analysis can estimate the frequency range of unstable poles.

The mutual interactions between L1N and L2N terminals can be investigated using (18). A change in the Load#3 (step change in i_{o3}) would act as disturbance not only to v_{o3}, but to all other converters. Theses mutual interactions can be observed by the analysis of $\triangle v_{o2}/\triangle i_{o3}$ or $\triangle v_{o3}/\triangle i_{o2}$.

In this case, the nominal power of Load#3 is increasing in steps of 4 kW, 6 kW, and 8 kW, while the nominal power of Load#2 is kept constant at 2 kW. The small-signal dynamics of $\triangle v_{o2}$ for step changes in $\triangle i_{o3}$ can be observed from step response analysis of $\boldsymbol{T}_{\rm MG}(2,3)$, which is presented in Fig. 10(a). The impact of $\triangle i_{o3}$ on $\triangle v_{o2}$ is rather insignificant, whereas, the impact of $\triangle i_{o2}$ on $\triangle v_{o3}$ is significant. A comparison between the step responses of $\triangle v_{o2}/\triangle i_{o3}$ and $\triangle v_{o3}/\triangle i_{o2}$ is shown in Fig. 10(b). This analysis shows that the control system of Load#3 is more liable to disturbances.

In order to further illustrate the interactions between L1N and L2N terminals, it is useful to apply Gershgorin circle

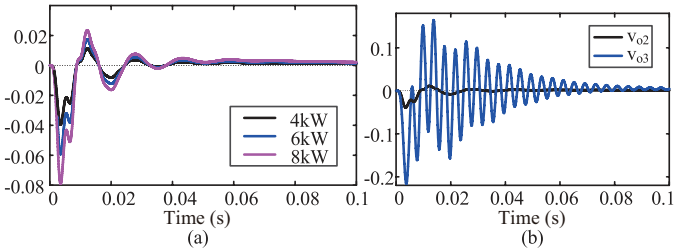

Fig. 10. Mutual interactions between L1N and L2N terminals: (a) the step response of $\triangle v_{o2}/\triangle i_{o3}$ for different operating points of Load#3, and (b) the step response of $\triangle v_{o2}/\triangle i_{o3}$ and $\triangle v_{o3}/\triangle i_{o2}$ for similar operating point.

theorem to the transfer matrix $\boldsymbol{T}_{\rm MG}$. The Gershgorin bands for diagonal elements of $\boldsymbol{T}_{\rm MG}$, including $\boldsymbol{T}_{\rm MG}(1,1)$, $\boldsymbol{T}_{\rm MG}(2,2)$, and $\boldsymbol{T}_{\rm MG}(3,3)$ are shown, respectively, in Figs. 11(a),(b), and (c). The Gershgorin bands are given for three loading conditions of the microgrid. First, the unbalance ratio Load#3/Load#2 is 200%. Then, this ratio increases to 300% and further to 400%. As it is presented in Fig. 11, with the increase of unbalance ratio, the coupling in MIMO system becomes weaker, i.e. the Gershgorin circles become thinner. Thus, when the bipolar dc microgrid is more unbalanced, the MIMO system given by (18) tends to be more diagonal, meaning that $\triangle v_{o1}$ is weakly affected by $\triangle i_{o2}$, $\triangle i_{o3}$, and $\triangle v_d$. This holds for other two outputs as well.

To further investigate the mutual interactions between the control loops of converters, the RGA analysis is applied to $\boldsymbol{T}_{\rm MG}(jw)$ at various frequencies. The RGA values of $\triangle v_{o3}$ for four inputs are shown in Fig. 12(a). Ideally, for a system with low level of interactions, the control loop of a local system only interacts with its local disturbance. For instance, the ideal case for $\triangle v_{o3}$ is that RGA values are one for $\triangle i_{o3}$ and they are zero for all other inputs ($\triangle i_{o2}$, $\triangle i_{o1}$, and $\triangle v_d$). However, as it is presented in Fig. 12(a), the control loop of $\triangle v_{o3}$ strongly interacts with $\triangle i_{o2}$ and $\triangle v_d$ for frequency range of 1 to 100 rad/s. This reveals that the voltage control loops of the converters connected to L1N are strongly affected by the currents of the converters connected to L2N bus, which is in fact the mutual interactions among control loops of converters. In case of $\triangle v_{o2}$, the control loop is mainly affected by its local disturbance $\triangle i_{o2}$, which is indicated in Fig. 12(b). For all frequencies, the highest RGA values belong to $\triangle i_{o2}$.

In the next stage, we investigate the frequency response of $\boldsymbol{T}_{\rm MG}(s)$ using SVD analysis. Note that the SVD analysis takes account of all interactions of inputs and outputs. The region of the singular values of $\boldsymbol{T}_{\rm MG}(jw)$ which is confined by $\overline{\sigma}_i$ and $\underline{\sigma}_i$ is shown in Fig. 13(a). This shows that for higher frequencies, if excited, the higher amplification of inputs would appear in the outputs. An interesting point of Fig. 13(a) is around frequencies between 1400 and 1800 rad/s. At this point, $\overline{\sigma}_i$ and $\underline{\sigma}_i$ begin to change abruptly. To better illustrate it, a condition number which is the ratio of $\overline{\sigma}_i$ / $\underline{\sigma}_i$ is defined.

For different unbalance ratios (200%, 300%, and 400%), the condition number defined above is presented in Fig. 13(b). For all unbalance ratios, the minimum condition number happens in frequency range of 1400 and 1800 rad/s. This is exactly the

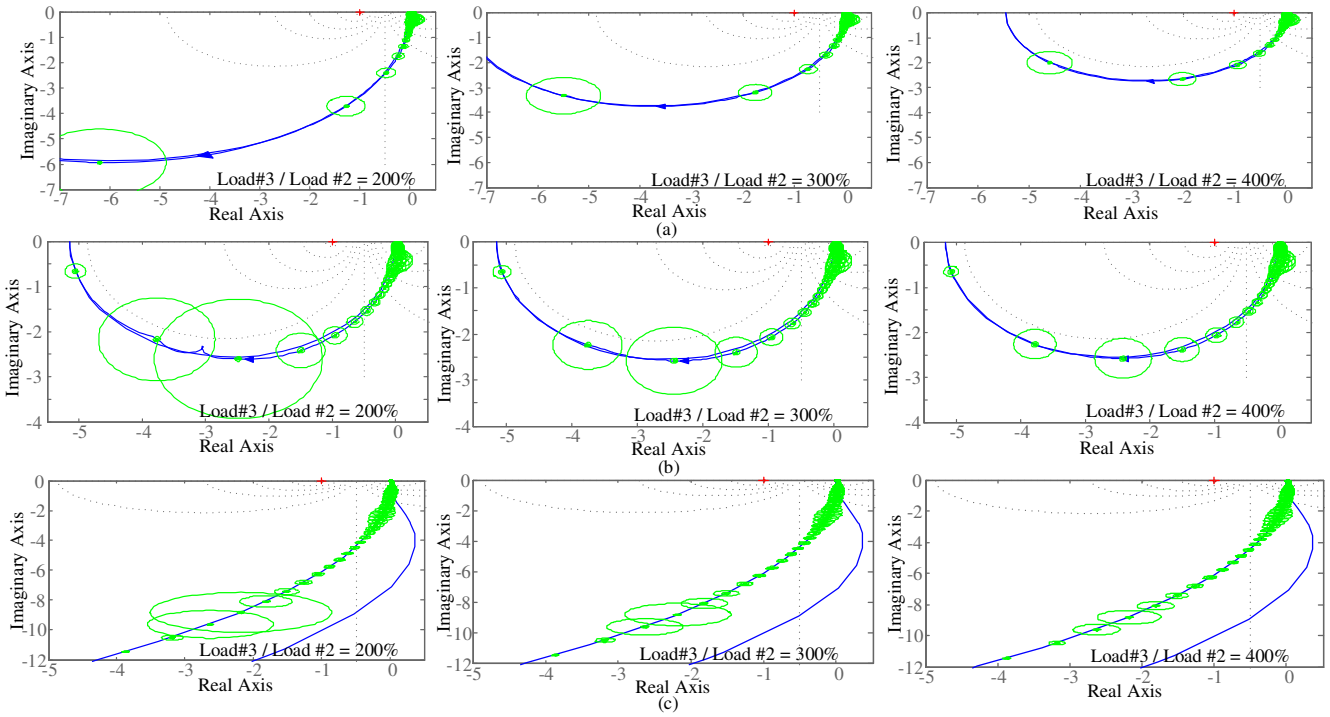

Fig. 11. Gershgorin circles indicating the degree of coupling in $\boldsymbol{T}_{\mathrm{MG}}(s)$, (a) $\boldsymbol{T}_{\mathrm{MG}}(1,1)$, (b) $\boldsymbol{T}_{\mathrm{MG}}(2,2)$, and (c) $\boldsymbol{T}_{\mathrm{MG}}(3,3)$.

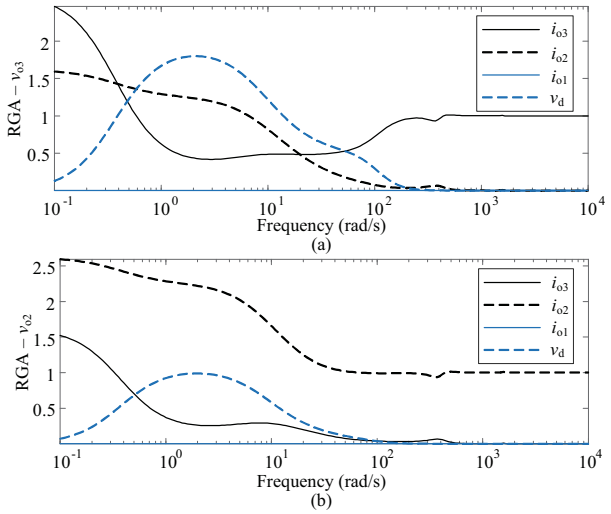

Fig. 12. RGA analysis (a) the RGA values for $v_{\mathrm{o}3}$, and (b) the RGA values for $v_{\mathrm{o}2}$

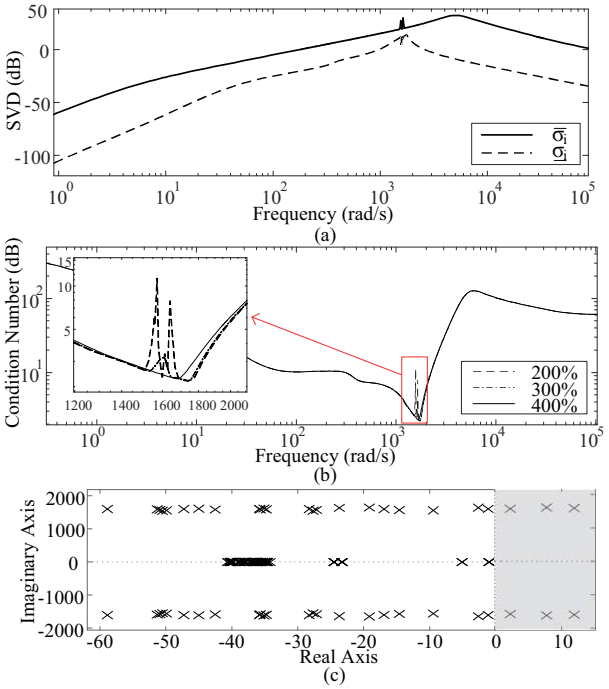

Fig. 13. SVD analysis, (a) maximum and minimum singular values of $\boldsymbol{T}_{\mathrm{MG}}(jw)$, (b) condition number $(\bar{\sigma}_i/\underline{\sigma}_i)$ for various unbalance ratios, and (c) the dominant poles of microgrid.

frequency of the unstable poles of $\boldsymbol{T}_{\mathrm{MG}}(jw)$ which is shown in Fig. 13(c). Therefore, the condition number resulted from SVD analysis can be regarded as a criteria to predict the frequency of unstable poles. It does not give information whether a system is stable or not; rather, it estimates the frequency of unstable poles while considers the mutual interactions.

B. The Impact of Voltage Balancer on Microgrid Stability

This study reveals that the dominant poles of the microgrid are significantly affected by the control system of the voltage balancer.

In this case, the Load#1, Load#2, and Load#3 consume the rated power of 10 kW, 2 kW, and 4 kW, respectively, and the voltage balancer has the following standard PI controller:

$$K_{\mathrm{p}}\left(1+\frac{1}{T_{\mathrm{i}}\,s}\right)$$

where K_{p} and T_{i} are proportional and integral coefficients. Note that we are only interested in revealing the significant

impact of voltage balancer's control system on the overall stability of bipolar dc microgrid and we have no intention to optimize the PI controller. Hence, for the ease of calculations, the coefficient $T_{\rm i}$ is assumed to be fixed at 0.01, while $k_{\rm p}$ would adopt three values including 10^{-2}, 10^{-3}, and 10^{-4}.

The dominant poles of $\boldsymbol{T}_{\rm MG}$ for three values of $K_{\rm p}$ are presented in Fig. 14(a). The poles belong to all input/output pairs. A change in $K_{\rm p}$ would remarkably shape the regions occupied by the poles. For $K_{\rm p}=10^{-2}$, the microgrid is unstable and many of dominant poles have positive real parts. With the decrease of $K_{\rm p}$ to 10^{-3}, majority of poles migrate to the left-half plane. However, the stability of microgrid is achieved at $K_{\rm p}=10^{-4}$. The remarkable impact of the balancer's control system on the system stability is also simplified and presented in Fig. 14(b). For smaller values for $K_{\rm p}$, the occupied regions by dominant poles shrink so the poles on the right-half plane move completely to the left-half plane. For further information, the step response of $\triangle v_{\rm o3}/\triangle i_{\rm o2}$ for three values of $K_{\rm p}$ is shown in Fig. 15.

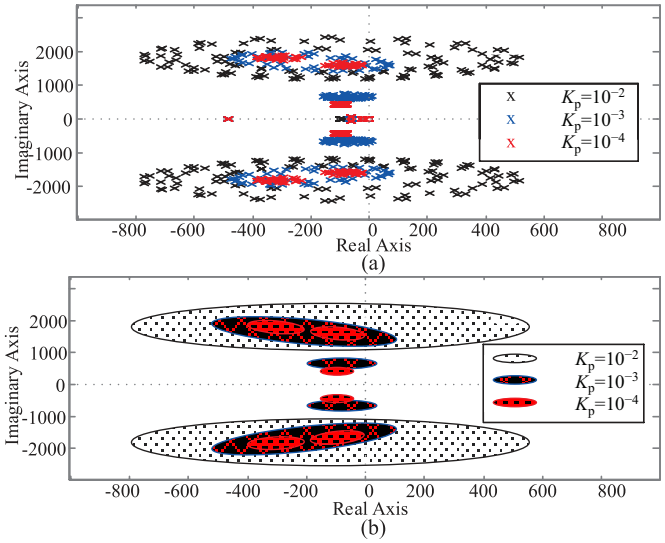

Fig. 14. Sensitivity analysis of $\boldsymbol{T}_{\rm MG}$ for changing the PI controller of the voltage balancer, (a) dominant poles of $\boldsymbol{T}_{\rm MG}$, and (b) occupied regions of the poles.

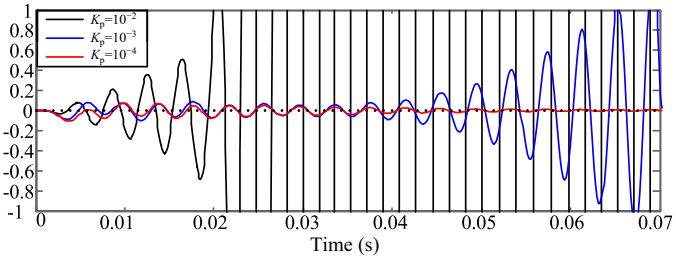

Fig. 15. The step response of $\triangle v_{\rm o3}/\triangle i_{\rm o2}$ for three values of $K_{\rm p}$.

Therefore, it can be concluded that the control system of the voltage balancer is a critical location to employ damping mechanisms. By adding active damping methods to the balancer's control system, or employing more robust controllers, such as predictive or adaptive controllers, the overall stability of microgrid can be effectively improved.

IV. Conclusion

This paper devises an MIMO modeling method to quantify the mutual interactions and small-signal stability of bipolar-type dc microgrids. By analyzing this MIMO system, the followings are concluded: 1) when a locally stable converter is connected to the microgrid, its control system can become unstable as the dominant poles are pushed to unstable region; 2) a load change on L1N bus impacts the output voltage of the converter connected to L2N bus; 3) the Gershgorin analysis reveals that the coupling between input-output pairs becomes weaker as the bipolar dc microgrid becomes more unbalanced; 4) the SVD analysis can be effectively utilized to calculate the frequency of unstable poles; and 5) the control system of the voltage balancer can significantly influence the overall stability of microgrid, so it is a perfect place to implement damping system. The MIMO model of the microgrid can be further used to tune control systems of converters and design an advanced controller for voltage balancer while providing desired damping to the system. In the broader scale, the stability of a cluster of bipolar dc microgrids can be investigated by connecting the MIMO models of individual microgrids.

References

[1] M. Hamzeh, M. Ghafouri, H. Karimi, K. Sheshyekani, and J. M. Guerrero, "Power oscillations damping in DC microgrids," *IEEE Transactions on Energy Conversion*, vol. 31, no. 3, pp. 970–980, Mar. 2016.

[2] S. Anand, B. G. Fernandes, and J. M. Guerrero, "Distributed control to ensure proportional load sharing and improve voltage regulation in low-voltage dc microgrids," *IEEE Transactions on Power Electronics*, vol. 28, no. 4, pp. 1900–1913, Apr. 2013.

[3] J. M. Guerrero, J. C. Vasquez, J. Matas, L. G. de Vicuna, and M. Castilla, "Hierarchical control of droop-controlled AC and DC microgrids—A general approach toward standardization," *IEEE Transactions on Industrial Electronics*, vol. 58, no. 1, pp. 158–172, Jan. 2011.

[4] H. Kakigano, Y. Miura, and T. Ise, "Low-voltage bipolar-type DC microgrid for super high quality distribution," *IEEE Transactions on Power Electronics*, vol. 25, no. 12, pp. 3066–3075, Dec. 2010.

[5] S. D. Tavakoli, J. Khajesalehi, M. Hamzeh, and K. Sheshyekani, "Decentralised voltage balancing in bipolar DC microgrids equipped with trans-z-source interlinking converter," *IET Renewable Power Generation*, vol. 10, no. 5, pp. 703–712, May 2016.

[6] X. J. Zhang, C. Y. Gong, and Z. L. Yao, "Three-level DC converter for balancing DC 800-V voltage," *IEEE Transactions on Power Electronics*, vol. 30, no. 7, pp. 3499–3507, Jul. 2015.

[7] M. B. Ferrera, S. P. Litrán, E. D. Aranda, and J. M. A. Márquez, "A converter for bipolar DC link based on SEPIC-Cuk combination," *IEEE Transactions on Power Electronics*, vol. 30, no. 12, pp. 6483–6487, Dec. 2015.

[8] J. Lago and M. L. Heldwein, "Operation and control-oriented modeling of a power converter for current balancing and stability improvement of DC active distribution networks," *IEEE Transactions on Power Electronics*, vol. 26, no. 3, pp. 877–885, Mar. 2011.

[9] Y. J. Gu, W. H. Li, and X. N. He, "Analysis and control of bipolar LVDC grid with DC symmetrical component method," *IEEE Transactions on Power Systems*, vol. 31, no. 1, pp. 685–694, Jan. 2016.

[10] S. D. Tavakoli, M. Mahdavyfakhr, M. Hamzeh, K. Sheshyekani, and E. Afjei, "A unified control strategy for power sharing and voltage balancing in bipolar DC microgrids," *Sustainable Energy, Grids and Networks*, vol. 11, pp. 58–68, Sep. 2017.

[11] S. Anand and B. G. Fernandes, "Reduced-order model and stability analysis of low-voltage DC microgrid," *IEEE Transactions on Industrial Electronics*, vol. 60, no. 11, pp. 5040–5049, Nov. 2013.

[12] A. P. N. Tahim, D. J. Pagano, E. Lenz, and V. Stramosk, "Modeling and stability analysis of islanded DC microgrids under droop control," *IEEE Transactions on Power Electronics*, vol. 30, no. 8, pp. 4597–4607, Aug. 2015.
[13] P. Magne, B. Nahid-Mobarakeh, and S. Pierfederici, "Dynamic consideration of DC microgrids with constant power loads and active damping system-A design method for fault-tolerant stabilizing system," *IEEE Journal of Emerging and Selected Topics in Power Electronics*, vol. 2, no. 3, pp. 562–570, Sep. 2014.
[14] G. Sulligoi, D. Bosich, G. Giadrossi, L. Zhu, M. Cupelli, and A. Monti, "Multiconverter medium voltage DC power systems on ships: Constant-power loads instability solution using linearization via state feedback control," *IEEE Transactions on Smart Grid*, vol. 5, no. 5, pp. 2543–2552, Sep. 2014.
[15] M. Su, Z. J. Liu, Y. Sun, H. Han, and X. C. Hou, "Stability analysis and stabilization methods of DC microgrid with multiple parallel-Connected DC-DC Converters Loaded by CPLs," *IEEE Transactions on Smart Grid*, vol. 9, no. 1, pp. 132–142, Jan. 2018.
[16] N. H. van der Blij, L. M. Ramirez-Elizondo, M. T. J. Spaan, and P. Bauer, "A state-space approach to modelling DC distribution systems," *IEEE Transactions on Power Systems*, vol. 33, no. 1, pp. 943–950, Jan. 2018.
[17] S. R. Huddy and J. D. Skufca, "Amplitude death solutions for stabilization of DC microgrids with instantaneous constant-power loads," *IEEE Transactions on Power Electronics*, vol. 28, no. 1, pp. 247–253, Jan. 2013.
[18] A. Kwasinski and C. N. Onwuchekwa, "Dynamic behavior and stabilization of DC microgrids with instantaneous constant-power loads," *IEEE Transactions on Power Electronics*, vol. 26, no. 3, pp. 822–834, Mar. 2011.
[19] A. M. Rahimi and A. Emadi, "An analytical investigation of DC/DC power electronic converters with constant power loads in vehicular power systems," *IEEE Transactions on Vehicular Technology*, vol. 58, no. 6, pp. 2689–2702, Jul. 2009.
[20] S. D. Tavakoli, G. Kadkhodaei, M. Mahdavyfakhr, M. Hamzeh, and K. Sheshyekani, "Interlinking converters in application of bipolar dc microgrids," in *Proceedings of the 8th Power Electronics, Drive Systems & Technologies Conference*, 2017.
[21] A. Yazdani and R. Iravani, *Voltage-Sourced Converters in Power Systems: Modeling, Control, and Applications*. New Jersey: Wiley-IEEE Press, 2010.

Saman Dadjo Tavakoli received his M.S. degree in Electrical Engineering from Shahid Beheshti University, Tehran, Iran, in 2015. He is working towards a Ph.D. degree in Electrical Engineering as an early-stage researcher as part of InnoDC (Innovative tools for offshore wind and DC grids) project at Polytechnic University of Catalonia (UPC), Barcelona, Spain. His research interests include multi-terminal HVDC systems, DC microgrids, power system stability, and advanced control system design.

Peng Zhang (M'07–SM'10) received the Ph.D. degree in Electrical Engineering from the University of British Columbia, Vancouver, BC, Canada, in 2009. He is a SUNY Empire Innovation Professor at Stony Brook University, NY, USA. He was a Francis L. Castleman Associate Professor and a Centennial Associate Professor at the University of Connecticut, Storrs, CT, USA, from 2017 to 2019. He was a System Planning Engineer at BC Hydro and Power Authority, Vancouver, during 2006-2010. His research interests include networked microgrids, programmable microgrids, cyber resilience, formal methods and quantum engineering.

Dr. Zhang is an individual member of CIGRÉ. He is an Editor for the IEEE Transactions on Power Systems, the IEEE Transactions on Sustainable Energy and the IEEE Power and Energy Society Letters, an Associate Editor for the IEEE Journal of Oceanic Engineering and the IEEE Transactions on Industrial Electronics.

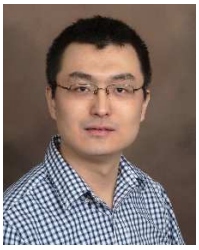

Xiaonan Lu (M'13) received his B.E. and Ph.D. degrees in Electrical Engineering from Tsinghua University, Beijing, China, in 2008 and 2013, respectively. From September 2010 to August 2011, he was a guest Ph.D. student at the Department of Energy Technology, Aalborg University, Denmark. From October 2013 to December 2014, he was a Postdoc Research Associate at the Department of Electrical Engineering and Computer Science, University of Tennessee, Knoxville. From January 2015 to July 2018, he was with Argonne National Laboratory, first as a Postdoc Appointee and then as an Energy Systems Scientist. In July 2018, he joined the College of Engineering in Temple University as an Assistant Professor.

Dr. Lu serves as the Associate Editor of IEEE Transactions on Industrial Electronics, the Associate Editor of IEEE Transactions on Industry Applications and the Editor of IEEE Transactions on Smart Grid. He also serves as the Secretary of Industrial Power Converters Committee (IPCC) in IEEE Industry Applications Society (IAS).

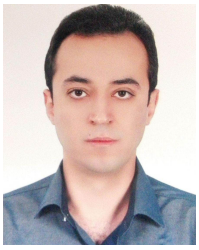

Mohsen Hamzeh received the B.Sc. and M.Sc. degrees from the University of Tehran, Tehran, Iran, in 2006 and 2008, respectively, and the Ph.D. degree from Sharif University of Technology, Tehran, Iran, in 2012, all in Electrical Engineering. From 2013 to 2018, he was an Assistant Professor with Shahid Beheshti University. In 2018, he joined the School of Electrical and Computer Engineering, University of Tehran. His research interests include renewable energies, microgrid control and applications of power electronics in power distribution systems.